Molecular Therapy
Original Article

Self-amplifying loop of NF-κB and periostin initiated by PIEZO1 accelerates mechano-induced senescence of nucleus pulposus cells and intervertebral disc degeneration

Jinna Wu,[1,5] Yuyu Chen,[1,5] Zhiheng Liao,[1,5] Hengyu Liu,[1] Shun Zhang,[1] Dongmei Zhong,[2] Xianjian Qiu,[3] Taiqiu Chen,[3] Deying Su,[4] Xiaona Ke,[1] Yong Wan,[1] Taifeng Zhou,[1,6] and Peiqiang Su[1,6]

[1]Department of Spine Surgery, Guangdong Provincial Key Laboratory of Orthopedics and Traumatology, The First Affiliated Hospital of Sun Yat-sen University, No.58 Zhongshan 2nd Road, Yuexiu District, Guangzhou 510080, China; [2]Institute of Precision Medicine, The First Affiliated Hospital of Sun Yat-sen University, Guangzhou 510080, China; [3]Department of Orthopedics, Sun Yat-sen Memorial Hospital of Sun Yat-sen University, Guangzhou 510120, China; [4]Guangdong Provincial Key Laboratory of Proteomics and State Key Laboratory of Organ Failure Research, School of Basic Medical Sciences, Southern Medical University, Guangzhou 510515, China

Abnormal mechanical load is a main risk factor of intervertebral disc degeneration (IDD), and cellular senescence is a pathological change in IDD. In addition, extracellular matrix (ECM) stiffness promotes human nucleus pulposus cells (hNPCs) senescence. However, the molecular mechanism underlying mechano-induced cellular senescence and IDD progression is not yet fully elucidated. First, we demonstrated that mechano-stress promoted hNPCs senescence via NF-κB signaling. Subsequently, we identified periostin as the main mechano-responsive molecule in hNPCs through unbiased sequencing, which was transcriptionally upregulated by NF-κB p65; moreover, secreted periostin by senescent hNPCs further promoted senescence and upregulated the catabolic process in hNPCs through activating NF-κB, forming a positive loop. Both *Postn* (encoding periostin) knockdown via siRNA and periostin inactivation via neutralizing antibodies alleviated IDD and NPCs senescence. Furthermore, we found that mechano-stress initiated the positive feedback of NF-κB and periostin via PIEZO1. PIEZO1 activation by Yoda1 induced severe IDD in rat tails without compression, and *Postn* knockdown alleviated the Yoda1-induced IDD *in vivo*. Here, we reported for the first time that self-amplifying loop of NF-κB and periostin initiated via PIEZO1 under mechano-stress accelerated NPCs senescence, leading to IDD. Furthermore, periostin neutralizing antibodies, which may serve as potential therapeutic agents for IDD, interrupted this loop.

INTRODUCTION

Intervertebral disc degeneration (IDD) is a chronic and multifactorial skeletal disease, considered as the leading cause of low back pain.[1–3] It is caused by an imbalance between anabolism and catabolism of the intervertebral disc (IVD), especially extracellular matrix (ECM) degradation of the nucleus pulposus (NP).[4–6] The IVD is a special cartilaginous organ connecting the adjacent vertebral bodies, consisting of the central NP and the outer annulus fibrosus (AF).[7,8] The IVD distributes mechanical load on the adjacent vertebral bodies,[9] and recent studies have shown that mechanical overload is a risk factor of IDD.[10–15] Evolutionarily, the upright posture is associated with a higher incidence of spine lesions in humans, compared with crawling mammals.[16] Frequent posture changes, fatigue load, and long-time sitting increase the risk of IDD, owing to elevated load on IVDs.[17] The NP senses and responds to mechanical stimuli, and ECM stiffness increases with aging and degeneration.[18] It is known that NP cells (NPCs) prefer a softer matrix (0.3 kPa),[19] while a stiffer matrix (25 kPa) leads to NPCs senescence.[20] However, the interplay between mechanics and biology during NPCs senescence and IDD progression has not yet been fully elucidated, and further elucidation of the underlying molecular mechanisms is needed.

Cellular senescence is a stable cell-cycle arrest, characterized by enhanced β-galactosidase (β-Gal) activity and the senescence-associated secretory phenotype (SASP).[21] Senescent cells were first detected in human IVDs by β-Gal staining, and NPCs senescence was positively related to IDD progression.[22] SASP is featured by the upregulation of pro-inflammatory factors such as interleukin-1β (IL-1β), IL-6, and IL-8, triggering inflammatory cascades and accelerating

Received 8 November 2021; accepted 21 May 2022;
https://doi.org/10.1016/j.ymthe.2022.05.021.

[5]These authors contributed equally

[6]Senior authors

Correspondence: Taifeng Zhou, Department of Spine Surgery, Guangdong Provincial Key Laboratory of Orthopedics and Traumatology, The First Affiliated Hospital of Sun Yat-sen University, No.58 Zhongshan 2nd Road, Yuexiu District, Guangzhou 510080, China.
E-mail: zhoutf7@mail.sysu.edu.cn
Correspondence: Peiqiang Su, Department of Spine Surgery, Guangdong Provincial Key Laboratory of Orthopedics and Traumatology, The First Affiliated Hospital of Sun Yat-sen University, No.58 Zhongshan 2nd Road, Yuexiu District, Guangzhou 510080, China.
E-mail: supq@mail.sysu.edu.cn

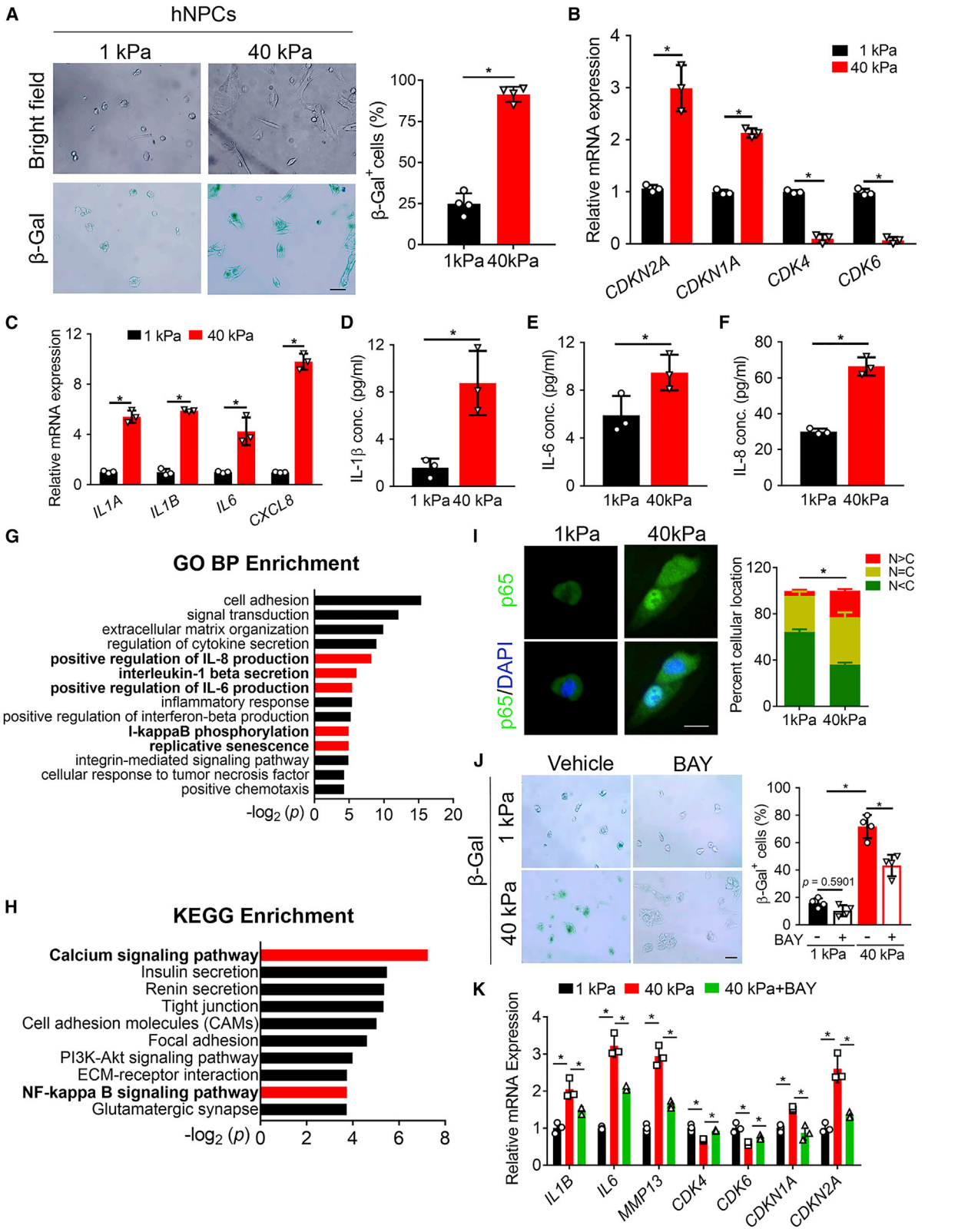

(legend on next page)

the development of IDD.[23,24] Recent studies showed that $p16^{Ink4a}$, a master regulator of cellular senescence,[25] was upregulated in the IVDs of IDD patients, and knockout of *Cdkn2a* (encoding $p16^{Ink4a}$) partially alleviated IDD in a tail suspension mouse model.[26] However, conditional knockout of *Cdkn2a* in IVD cells did not attenuate age-dependent IDD in mice,[23] indicating that cellular senescence and SASP might play a more important role in mechano-induced IDD. Thus, a more profound understanding of the regulatory mechanisms underlying cellular senescence and SASP contributing to IDD progression might provide new targets for IDD therapy.

Periostin (encoded by *POSTN*) was first identified in the periodontal ligament and periosteum of adult mice.[27] It is predominantly expressed in connective tissues sensing mechanical load, such as heart valves, skin, periodontal ligaments, tendons, and bones.[28] It is a mechano-responsive molecule involved in skin wound healing processes[29] and maintenance of periodontium integrity.[30] Recently, it was reported that the expression of *POSTN* was significantly increased in the IVDs of IDD patients,[31] suggesting a potential role of periostin in IDD progression, but the regulatory function of periostin in IDD has not been experimentally examined.

In this study, unbiased mRNA sequencing and assay for transposase-accessible chromatin sequencing (ATAC-seq) were employed to examine the changes of human NP cells (hNPCs) under mechano-stress conditions, and positive feedback of periostin and NF-κB p65 was identified as a key regulator involved in accelerating NPCs senescence and IDD progression. We also found that periostin knockdown by small interfering RNA (siRNA) or inactivation by neutralizing antibodies attenuated the progression of NPCs senescence and IDD progression *in vitro* and *in vivo*. Furthermore, we demonstrated that the positive loop was initiated by ECM stiffness via PIEZO1-Ca^{2+} to promote cellular senescence and IDD progression *in vitro* and *in vivo*.

RESULTS

Mechano-stress promotes hNPCs senescence and SASP via NF-κB p65

To examine how stiff ECM promoted hNPCs senescence and SASP, we seeded hNPCs on hydrogels with different stiffness (1 and 40 kPa) for 24 h, and then performed β-Gal staining to label senescent cells. As expected, hNPCs on stiff hydrogels (40 kPa) showed a more spreading cell morphology and more $\beta\text{-Gal}^+$ senescent cells compared with hNPCs on soft hydrogels (Figure 1A). The senescence markers *CDKN2A* (encoding p16) and *CDKN1A* (encoding p21) were upregulated in 40 kPa hNPCs, and *CDK4* and *CDK6* expression were downregulated (Figure 1B), suggesting cell-cycle arrest in 40 kPa hNPCs. Then, we examined the mRNA expression of *IL1A*, *IL1B*, *IL6*, and *CXCL8* (encoding IL-8) by qPCR, and the concentrations of IL-1β, IL-6, and IL-8 in cell culture medium by ELISA. These cytokines were significantly upregulated in 40 kPa hNPCs (Figures 1C–1F), indicating matrix stiffness promoted SASP of hNPCs as well.

Next, to explore the underlying molecular mechanisms, mRNA from hNPCs cultured on different hydrogels was collected for unbiased sequencing. Differentially expressed genes with fold change > 8 and $p < 0.05$ were analyzed by Gene Ontology (GO) term enrichment analysis in the biological processes (BP) category and Kyoto Encyclopedia of Genes and Genomes (KEGG) pathway enrichment analysis. GO term mapping of upregulated genes in 40 kPa hNPCs showed that IL-1β secretion, replicative senescence, and I-kappaB phosphorylation were upregulated (Figure 1G). Meanwhile, KEGG pathway enrichment analysis of upregulated genes in 40 kPa hNPCs suggested that the calcium signaling pathway and the NF-κB signaling pathway were highly upregulated (Figure 1H). To confirm the increased activity of the NF-κB signaling pathway in 40 kPa hNPCs, immunostaining of NF-κB p65 was performed. As expected, stiff hydrogels promoted NF-κB p65 translocation into the nucleus, indicating higher NF-κB p65 activity (Figure 1I). Last, we treated hNPCs on different hydrogels with BAY 11–7085 (BAY), an inhibitor of NF-κB signaling, and found that BAY significantly reduced the number of $\beta\text{-Gal}^+$ senescent cells and mRNA expression of the senescence markers *CDKN2A* and *CDKN1A*, and SASP markers *IL1B* and *IL6*, but increased *CDK4* and *CDK6* expression on stiff hydrogels (Figures 1J and 1K). Together, these data suggested that mechano-stress promoted hNPCs senescence and SASP via NF-κB p65.

Mechano-stress upregulates the transcription of *POSTN* via NF-κB p65

Among the cytokines and secretory proteins upregulated by high matrix stiffness, we noticed that *POSTN* expression increased most

Figure 1. Mechano-stress promotes hNPCs senescence and SASP via NF-κB p65

(A) Representative bright field (upper) and β-Gal staining (bottom) images of hNPCs cultured on indicated hydrogels for 24 h (left panel), and quantitation of $\beta\text{-Gal}^+$ senescent cells (right panel). n = 4 biologically independent samples. Scale bar, 100 μm. (B and C) Relative mRNA expression of the senescence markers (B) and SASP markers (C). Values were presented as the fold change compared with the 1 kPa group. n = 3 biologically independent samples. (D–F) Concentrations of IL-1β (D), IL-6 (E), and IL-8 (F) in the cell culture medium as determined by ELISA. n = 3 biologically independent samples. (G and H) GO term enrichment analysis in the biological process category (G) and KEGG pathway enrichment analysis (H) of upregulated genes in 40 kPa hNPCs compared with 1 kPa hNPCs. The bars marked in red were the ones we focused on. (I) Immunostaining of NF-κB p65 (green) in hNPCs cultured on indicated hydrogels for 24 h (left panel). DAPI (blue) indicated nuclei. Quantification of p65 localization was presented as mean ± SD (right panel). N < C, less NF-κB p65 in nucleus than in cytoplasm. N = C, similar levels of NF-κB p65 in cytoplasm and nucleus. N > C, more NF-κB p65 in nucleus than in cytoplasm. Three fields were randomly selected for each biological replicate. In total, 205 cells from the 1 kPa group and 174 cells from the 40 kPa group were analyzed. *Represents the statistical analysis was conducted in terms of the proportion of N > C between the two groups and $p < 0.05$. n = 3 biologically independent samples. Scale bar = 25 μm. (J) Representative β-Gal staining images of hNPCs cultured under indicated conditions for 24 h (left panel), and quantitation of $\beta\text{-Gal}^+$ senescent cells (right panel). BAY, BAY 11–7085. n = 4 biologically independent samples. Scale bar, 100 μm. (K) Relative mRNA expression of the matrix metabolism, senescence, and SASP markers was measured in hNPCs cultured under indicated conditions for 24 h. n = 3 biologically independent samples. Data were presented as the mean ± SD. *$p < 0.05$.

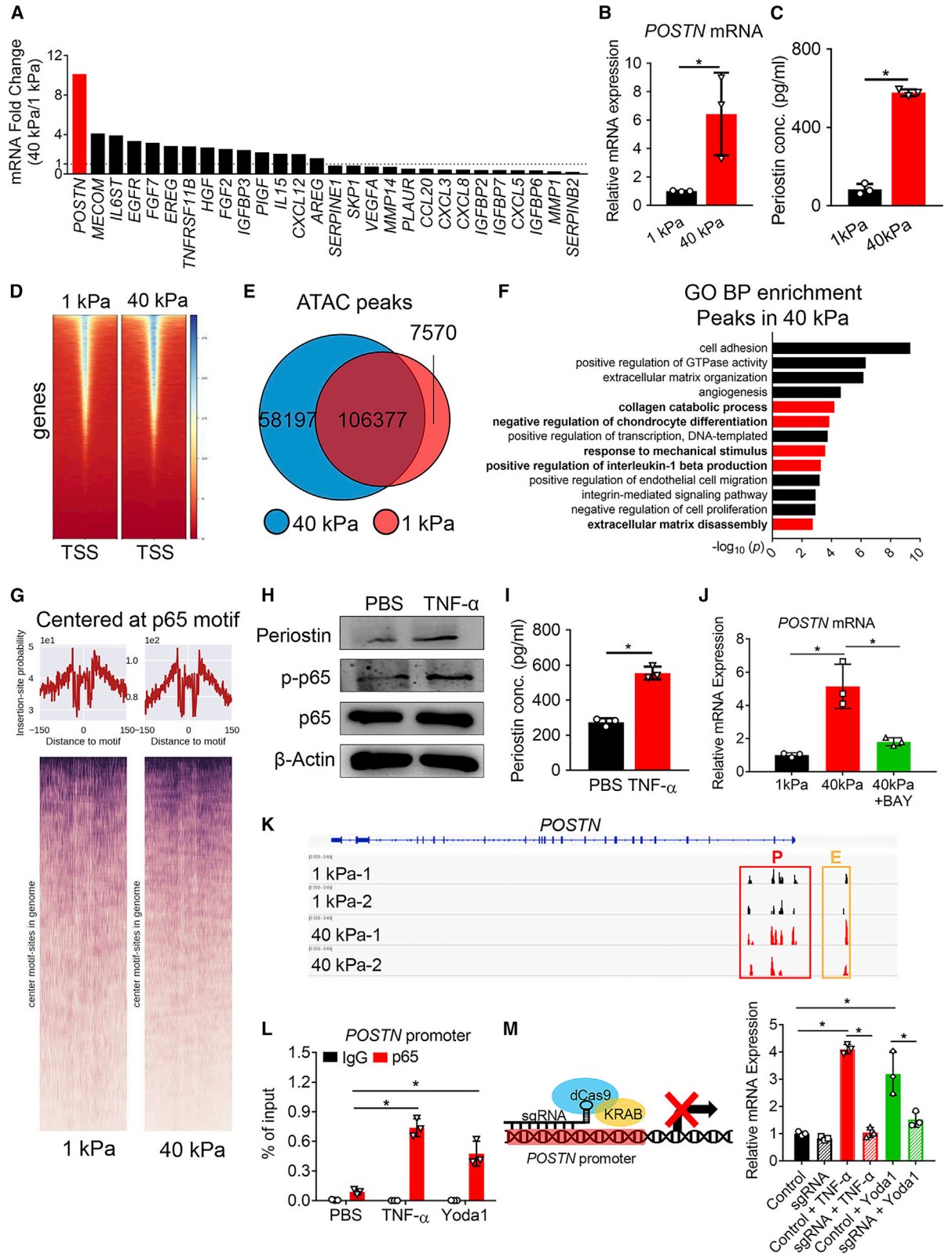

(legend on next page)

(Figure 2A and Figure S1). We then examined *POSTN* expression and periostin secretion of hNPCs on different hydrogels by qPCR and ELISA. *POSTN* mRNA expression of 40 kPa hNPCs was increased significantly (Figure 2B), and the periostin concentration in cell culture medium was also highly upregulated (Figure 2C). Since chromatin remodeling occurs during senescence,[32] we next investigated the underlying mechanism using a genome-wide approach. ATAC-seq was used to determine chromatin accessibility in hNPCs on different hydrogels. The number of ATAC-seq peaks increased in the 40 kPa hNPCs (Figures 2D and 2E), and GO BP term mapping of genes with a transcriptional start site (TSS) at the unique ATAC peaks of the 40 kPa hNPCs showed that collagen catabolic process, negative regulation of chondrocyte differentiation, and ECM disassembly were upregulated (Figure 2F). To identify NF-κB p65-mediated gene regulation, we tested whether chromatin was more accessible around the NF-κB p65 binding sites in 40 kPa hNPCs. NF-κB p65 motifs were assessed in all ATAC peaks, showing that ATAC-seq signal intensities were higher around NF-κB p65 motif in 40 kPa hNPCs (Figure 2G). Together, our ATAC-seq data analysis supported the notion that NF-κB p65 transcription activity in 40 kPa hNPCs was activated.

In addition, to confirm that NF-κB p65 promoted periostin expression, hNPCs were treated with tumor necrosis factor (TNF)-α. TNF-α treatment increased the phosphorylation level of NF-κB p65 and upregulated the expression and secretion of periostin, as examined by immunoblotting and ELISA (Figures 2H and 2I). Next, to investigate whether mechano-stress induced *POSTN* expression via NF-κB p65, we examined the *POSTN* expression level of BAY-treated 40 kPa hNPCs and found that BAY treatment abolished the mechano-induced *POSTN* expression (Figure 2J). Moreover, we observed that ATAC-seq signal intensities of 40 kPa hNPCs were strongly enhanced at the *POSTN* promoter and enhancer (https://www.ensembl.org/), in agreement with the upregulation of *POSTN* expression, suggesting that the chromatin comprising *POSTN*-regulatory regions was more accessible in 40 kPa hNPCs compared with 1 kPa hNPCs (Figure 2K). To test whether *POSTN* was a direct transcriptional target of NF-κB p65 in hNPCs, the *POSTN* promoter and enhancer were further analyzed, and an NF-κB p65 binding site in the promoter was predicted based on the ATAC-seq results and JASPAR (http://jaspar2016.genereg.net/). To determine whether the predicted NF-κB p65 binding site was required for *POSTN* expression under mechano-stress, we conducted chromatin immunoprecipitation (ChIP)-qPCR analysis using anti-NF-κB p65, where immunoglobulin (Ig) G served as a negative control. As shown in Figure 2L, activation of NF-κB p65 via TNF-α increased the binding of NF-κB p65 to the *POSTN* promoter. Furthermore, the NF-κB p65 binding site in the *POSTN* promoter region was functionally inhibited by targeting a nuclease-deficient (d) Cas9-Krüppel associated box (KRAB) fusion protein (dCas9-KRAB) to the NF-κB p65 binding site with small guide RNA (sgRNA) via lentivirus infection. Targeting dCas9-KRAB to putative enhancers or promoters recruits the H3K9 methyltransferase SET domain bifurcated histone lysine methyltransferase 1 (SETDB1), which increases local H3K9me3 binding and represses target gene expression.[33] As expected, dCas9-KRAB guided by sgRNA targeting the NF-κB p65 binding site in the *POSTN* promoter greatly reduced *POSTN* expression under TNF-α treatment (Figure 2M). In addition, we generated a luciferase reporter construct driven by the *POSTN* promoter (Figure S2B) and performed a dual-luciferase reporter assay. TNF-α treatment increased the luciferase activity, while NF-κB p65 knockdown by specific siRNAs abolished these increases (Figures S2A and S2C). Together, these data demonstrated that *POSTN* was a direct transcriptional target of NF-κB p65 under mechanical stimuli.

Self-amplifying loop of NF-κB and periostin accelerates hNPCs senescence

Our data showed that mechano-stress prompted hNPCs to secrete periostin. We next investigated whether the secreted periostin in turn accelerated hNPCs senescence. hNPCs were treated with 1 μg/mL recombinant human periostin (rhPeriostin) for 24 h, and β-Gal staining showed that rhPeriostin significantly promoted hNPCs senescence (Figure 3A). The SASP was also upregulated by rhPeriostin, as indicated by the increase of *IL1A*, *IL1B*, and *IL6* expression (Figure 3B). Meanwhile, rhPeriostin decreased the expression of the anabolic markers *COL2A1* and *ACAN* and increased the expression of the catabolic marker *MMP13* (Figures 3C and 3D). Together, these data demonstrated that periostin promoted hNPCs senescence. Interestingly, rhPeriostin treatment increased the expression of periostin (Figure 3D, red arrow indicated the endogenous periostin). Moreover, rhPeriostin upregulated the phosphorylated p65 (p-p65) level (Figure 3D) and promoted p65 nuclear translocation (Figures 3H and 3J), suggesting that periostin increased NF-κB p65 activity to promote periostin expression in hNPCs. BAY

Figure 2. Mechano-stress upregulates the transcription of *POSTN* via NF-κB p65

(A) mRNA fold changes of cytokines and secretory proteins expression in 40 kPa hNPCs compared with 1 kPa hNPCs according to the mRNA-seq results. (B) qPCR result of *POSTN* in 1 kPa and 40 kPa hNPCs. n = 3 biologically independent samples. (C) Concentration of periostin in the cell culture medium as determined by ELISA. n = 3 biologically independent samples. (D) ATAC-seq signal intensities near transcriptional start sites (TSS). (E) Venn diagram showing the number of ATAC-seq peaks detected in 1 kPa or 40 kPa hNPCs. (F) GO term enrichment analysis in the biological process category of genes with TSS present in the unique ATAC peaks of the 40 kPa hNPCs. The bars marked in red were the ones we focused on. (G) ATAC-seq signal intensities near p65 motif. (H) Immunoblotting of periostin, p-p65 and p65 in hNPCs cultured under indicated treatment for 48 h. (I) Concentration of periostin as determined by ELISA in the cell culture medium of hNPCs under indicated treatments for 24 h. n = 3 biologically independent samples. (J) *POSTN* mRNA expression was measured in hNPCs cultured under indicated treatments for 24 h. n = 3 biologically independent samples. (K) ATAC peaks at promoter and enhancer regions of the *POSTN* locus. P, promoter; E, enhancer. (L) ChIP-qPCR assay was performed with anti-NF-κB p65 using hNPCs treated with PBS, TNF-α, or Yoda1 for 24 h to identify the binding between NF-κB p65 and the *POSTN* promoter. n = 3 biologically independent samples. (M) *POSTN* expression in hNPCs under indicated conditions. The NF-κB p65 binding site in the *POSTN* promoter region was occupied by dCas9-KRAB. Left panel: schematics of dCas9-KRAB. n = 3 biologically independent samples. Data are presented as the mean ± SD. *p < 0.05.

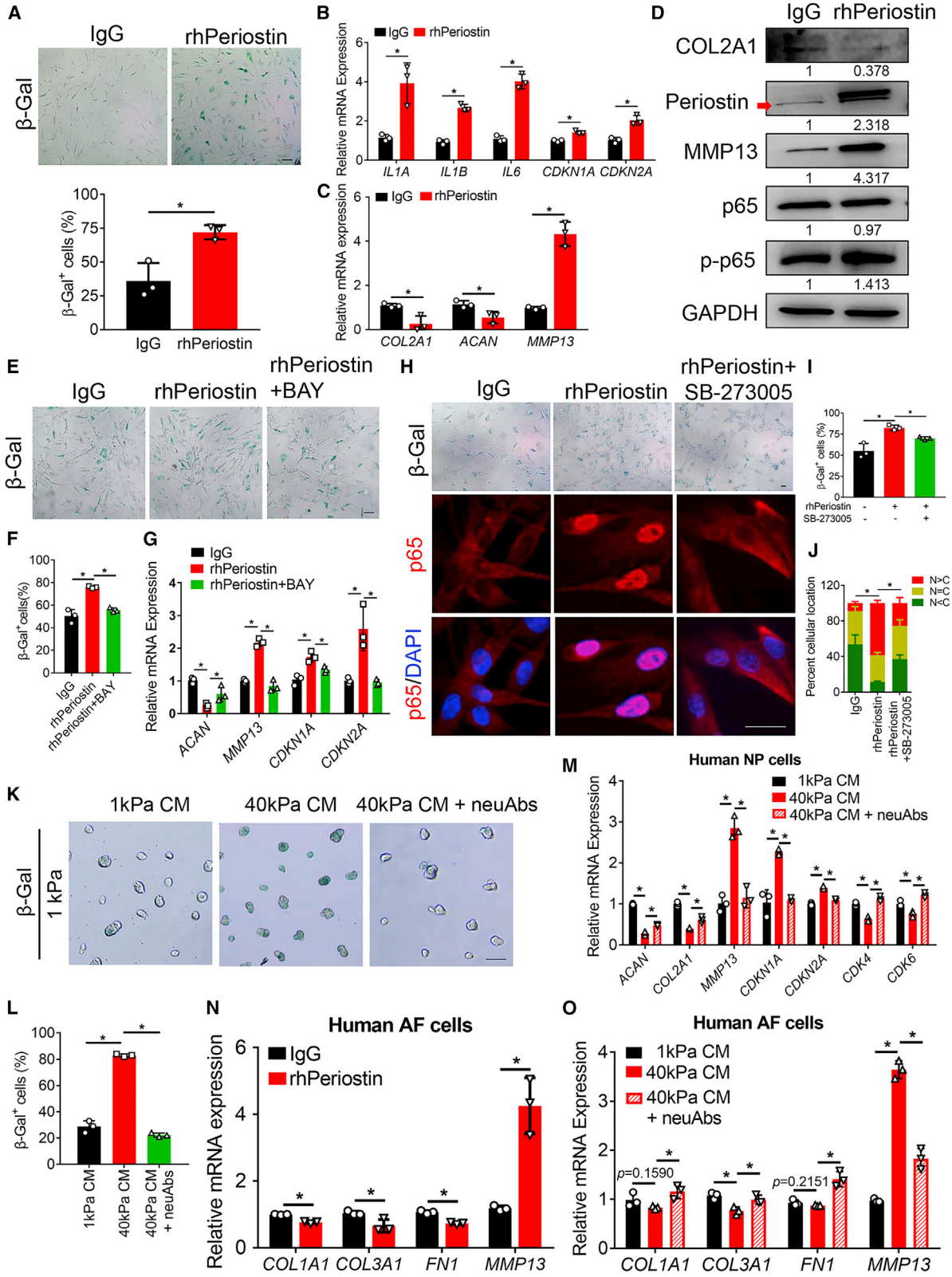

(legend on next page)

alleviated the rhPeriostin-induced increase of β-Gal$^+$ senescent cells (Figures 3E and 3F), and abolished the upregulation of *MMP13* expression (Figure 3G). Together, these data demonstrated that NF-κB and periostin formed a positive feedback loop that accelerated hNPCs senescence. Because integrin αVβ3 is the receptor of periostin, we next investigated whether periostin activated NF-κB and accelerated hNPCs senescence via integrin αVβ3 by using the integrin αVβ3 antagonist SB-273005. SB-273005 reduced the increase of β-Gal$^+$ senescent cells (Figures 3H and 3I) and abolished the rhPeriostin-induced nuclear localization of NF-κB p65 (Figures 3H and 3J). These data suggested that periostin interacted with integrin αVβ3 to activate NF-κB p65 and accelerate hNPCs senescence.

Subsequently, to examine whether periostin secreted by hNPCs under mechano-stress accelerated hNPCs senescence, we collected the cell culture medium of 40 kPa hNPCs as conditioned medium (CM). As expected, 40 kPa CM promoted 1 kPa hNPCs senescence (Figures 3K–3M). Periostin neutralizing antibodies (neuAbs) were used to further confirm that periostin in CM accelerated hNPCs senescence. β-Gal staining showed that periostin neuAbs alleviated 1 kPa hNPCs senescence induced by 40 kPa CM (Figures 3K and 3L), indicating it was periostin secreted by 40 kPa hNPCs that accelerated hNPCs senescence.

Since AF breakdown is a feature of IDD, we then investigated whether periostin secreted by hNPCs disturbed the matrix homeostasis of human AF cells. rhPeriostin decreased the expression of the anabolic markers (*COL1A1*, *COL3A1*, and *FN1*) and increased the expression of the catabolic marker *MMP13* (Figure 3N). Moreover, 40 kPa CM treatment increased *MMP13* expression and downregulated the expression of the anabolic markers (*COL1A1*, *COL3A1*, and *FN1*) in human AF cells (Figure 3O) compared with 1 kPa CM treatment. Furthermore, periostin neuAbs reversed the effects of 40 kPa CM on human AF cells (Figure 3O). Together, these data demonstrated that SASP of hNPCs induced by mechano-stress further disturbed the homeostasis of human AF cells, contributing to IDD progression.

Targeting periostin attenuates IDD *in vivo*

To probe the correlation between IDD progression and the positive feedback of NF-κB and periostin, we examined the expression of periostin, total p65, and p-p65 in human NP tissues by immunoblotting. The expression of periostin and p-p65 was highly increased in the degenerated human NP tissues compared with control tissues (Figure 4A). Furthermore, the immunohistochemistry (IHC) score of periostin increased with the increase of degeneration grade (Figures 4B and 4C), and periostin expression was also correlated positively with NF-κB p65 expression (Figure 4D), indicating a positive correlation among NF-κB, periostin, and IDD progression *in vivo*.

Next, a mechano-induced IDD rat model was generated (Figure 4E) 3 days after knocking down *Postn* by a specific siRNA delivered via AAV2 to explore whether periostin was a potential therapeutic target for IDD treatment. MRI showed that 2-week mechanical load led to severe disc degeneration in rat tails, while *Postn* knockdown attenuated the degenerative phenotype (Figure 4E). Disc degeneration was evaluated according to the Pfirrmann grading system, in which higher grades indicated more severe degeneration. The discs were degraded quickly under mechano-stress, and *Postn* knockdown alleviated the degeneration significantly (Figure 4F). After mechanical pressure, disc heights decreased and the proteoglycan levels in NP reduced; these effects were alleviated by *Postn* knockdown, as indicated by H&E staining and Safranin O staining (Figure 4G). Expression of the senescence marker p16 was also increased in the IDD rat model, while *Postn* knockdown reversed this effect (Figure 4H). Moreover, mechano-stress upregulated periostin and NF-κB p65 expression, as well as NF-κB p65 nuclear localization, and these effects were reversed by *Postn* knockdown in rat NP (Figures 4I–4K). These data demonstrated that targeting periostin attenuated IDD *in vivo* and inspired us to explore the potential benefits of periostin neutralizing antibodies in IDD therapy. Periostin neutralizing antibodies were injected locally into rat tails during mechano-stress. MRI showed that periostin neutralizing antibodies significantly attenuated

Figure 3. Self-amplifying loop of NF-κB and periostin accelerates hNPCs senescence

(A) Representative β-Gal staining images (top) of hNPCs treated with IgG or 1 μg/mL rhPeriostin for 24 h, and quantitation of β-Gal$^+$ senescent cells (bottom). n = 3 biologically independent samples. Scale bar, 100 μm. (B and C) Relative mRNA expression of the senescence and SASP markers (B) and matrix metabolism markers (C) as determined by qPCR in hNPCs treated with IgG or rhPeriostin for 24 h. n = 3 biologically independent samples. (D) Immunoblotting of periostin, p-p65, p65, COL2A1, and MMP13 in hNPCs treated with IgG or rhPeriostin for 24 h. The red arrow indicates endogenous periostin. Densitometry results were expressed as fold change in protein levels compared with IgG treated hNPCs after normalized to GAPDH. (E and F) Representative β-Gal staining images (E) of hNPCs cultured under indicated conditions for 24 h, and quantitation of β-Gal$^+$ senescent cells (F). n = 3 biologically independent samples. Scale bar, 100 μm. (G) Relative mRNA expression of the matrix metabolism and senescence markers as determined by qPCR in hNPCs cultured under indicated conditions. n = 3 biologically independent samples. (H) Representative β-Gal staining images (upper) of hNPCs treated with indicated conditions for 24 h and immunostaining images (middle and bottom) of NF-κB p65 (red) in hNPCs under indicated treatments for 30 min. DAPI (blue) indicates nuclei. Scale bar, 25 μm. (I) Quantitation of β-Gal$^+$ senescent cells in (H). n = 3 biologically independent samples. (J) Quantification of p65 localization in H, presented as mean ± SD. In total, 308, 200, and 281 cells were analyzed in the IgG, rhPeriostin, and rhPeriostin and SB-273005 groups, respectively. *Represents the statistical analysis was conducted in terms of the proportion of N > C among the three groups and $p < 0.05$. n = 3 biologically independent samples. (K and L) Representative β-Gal staining images (K) of hNPCs treated with indicated conditional medium or neutralizing antibodies for 24 h, and quantitation of β-Gal$^+$ senescent cells (L). CM, conditioned medium; neuAbs, periostin neutralizing antibodies. n = 3 biologically independent samples. Scale bar, 100 μm. (M) qPCR results of hNPCs treated with conditioned medium or neutralizing antibodies. n = 3 biologically independent samples. (N) Expression of the matrix metabolism markers as determined by qPCR in human AF cells treated with IgG or rhPeriostin for 24 h. n = 3 biologically independent samples. (O) Expression of the matrix metabolism markers as determined by qPCR in human AF cells treated with indicated conditioned medium from hNPCs or neutralizing antibodies for 24 h. n = 3 biologically independent samples. Data are presented as the mean ± SD. *$p < 0.05$.

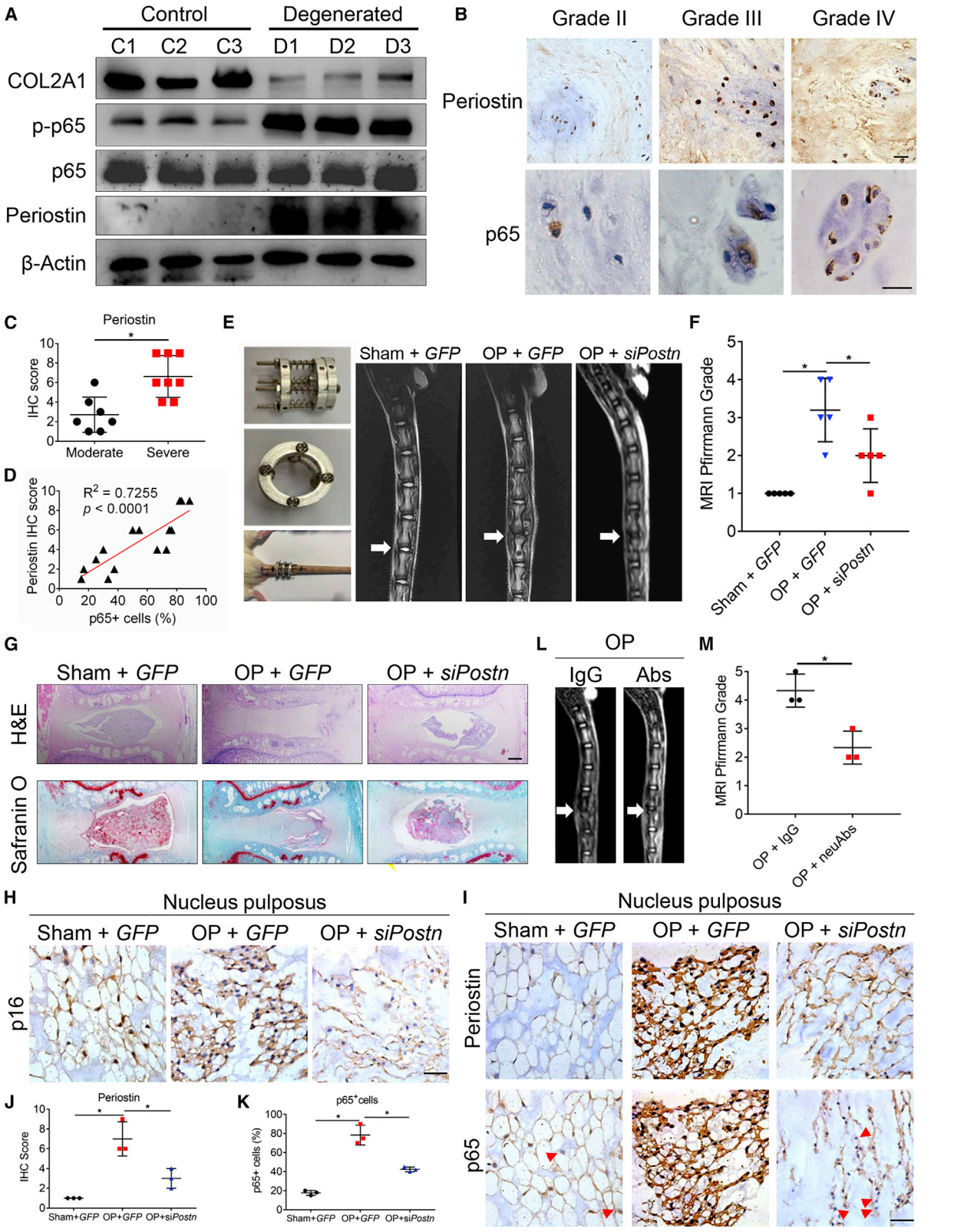

(legend on next page)

disc degeneration (Figures 4L and 4M). Together, these data demonstrated that periostin might serve as a new therapeutic target for IDD treatment.

Mechano-stress initiates the positive loop of NF-κB and periostin via PIEZO1

The mechanisms by which mechano-stress triggered the positive loop of NF-κB and periostin in hNPCs remained unknown. PIEZO1 is a well-characterized mechanosensitive channel that is involved in processes as diverse as skeletal development and NPCs senescence.[20,34] Thus, we explored whether PIEZO1 mediated the initiation of the positive loop. First, we examined the expression of PIEZO1 in human NP tissues by immunoblotting. PIEZO1 expression was increased in degenerated NP compared with control NP tissues, and PIEZO1 was hardly detected in control NP tissues (Figure 5A). Then, to test whether PIEZO1 functioned in normal hNPCs, Ca^{2+} flux was detected and imaged using Fluo-8 AM, of which fluorescence significantly increased if intracellular Ca^{2+} levels increase. Yoda1, a specific activator of PIEZO1, induced Ca^{2+} influx in hNPCs, which reached peaks quickly after treatment (Figure 5B and Video S1), suggesting that PIEZO1 functioned in hNPCs. Next, relative intracellular Ca^{2+} levels in hNPCs on different hydrogels were detected via Fluo-8 AM, and images were taken under the same parameters (exposure time and contrast ratio); 40 kPa hNPCs showed more fluorescence compared with 1 kPa hNPCs (Figure 5C), indicating higher intracellular Ca^{2+} levels in 40 kPa hNPCs. Together, these data indicated that PIEZO1 was expressed in hNPCs and perceived matrix stiffness changes.

Subsequently, we examined the role of PIEZO1 in the self-amplifying loop of NF-κB and periostin. Yoda1 increased the number of β-Gal^{+} senescent cells (Figure 5D), upregulated the expression of *CDKN1A* and *CDKN2A*, and decreased the expression of *CDK4* and *CDK6* (Figure 5E), suggesting PIEZO1 activation in hNPCs promoted senescence. Moreover, Yoda1 upregulated the expression of the SASP markers *IL1A*, *IL1B*, and *IL6* and catabolic markers *MMP3* and *MMP13*, and decreased the expression of the anabolic marker *COL2A1* (Figures 5F and 5G). Moreover, Yoda1 promoted NF-κB p65 nuclear localization (Figures 5H and 5I), indicating higher NF-κB activity, and increased periostin expression (Figure 5J). Furthermore, co-treatment with Yoda1 and BAY abolished Yoda1-induced periostin expression (Figure S3). In addition, Yoda1 treatment promoted NF-κB p65 binding to the *POSTN* promoter (Figure 2L), and dCas9-KRAB guided by sgRNA targeting the NF-κB p65 binding site in *POSTN* promoter greatly reduced *POSTN* expression under Yoda1 treatment (Figure 2M). NF-κB p65 knockdown diminished the increased luciferase activity under Yoda1 treatment (Figures S2A and S2C). Taken together, our results indicated that Yoda1 induced periostin expression via NF-κB p65. Then GsMTx4, a gating modifier peptide from spider venom, was used to block the activation of PIEZO1.[35,36] PIEZO1 inhibition by GsMTx4 reduced the number of β-Gal^{+} senescent cells in 40 kPa hNPCs (Figures 5K and 5L) and reversed the matrix stiffness-induced increase in expression of the catabolic marker *MMP13* and *POSTN* (Figure 5M). To examine whether PIEZO1 activation initiated the positive loop and caused IDD *in vivo*, 5 μmol/kg Yoda1 was injected locally into rat tails 3 days after AAV2-si*Postn* injection. MRI showed that Piezo1 activation by Yoda1 led to severe disc degeneration in rat tails even without mechanical pressure, and *Postn* knockdown significantly reversed this Yoda1-induced effect *in vivo* (Figures 5N and 5O). Taken together, these data demonstrated that mechano-stress initiated the self-amplifying loop of NF-κB and periostin via PIEZO1.

DISCUSSION

Excessive mechanical load on the NP is known to exacerbate IDD progression, and ECM stiffness is a main mechanical factor that the NP perceives.[37] ECM stiffness in the NP increases with aging and grade of the degeneration,[18] and plays a crucial role in maintaining NP homeostasis. Soft ECM (0.3 kPa) regulated the clustered morphology and helped the NP maintain a healthy condition,[19] and a recent study showed that 25 kPa hydrogels promoted hNPCs senescence compared with 1 kPa hydrogels.[20] However, how the mechanics promoted hNPCs senescence and the following biological processes were not yet fully elucidated. Through unbiased high-throughput sequencing, we confirmed that hNPCs preferred a soft ECM, and matrix stiffness promoted hNPCs senescence as well as SASP, which was consistent with previous studies. Furthermore, we illustrated that mechano-stress promoted hNPCs senescence via NF-κB p65, because NF-κB p65 inhibition by BAY reduced the increase of senescent hNPCs on stiff matrix.

We for the first time identified periostin as a key player in the acceleration of hNPCs senescence under mechano-stress. Periostin is a matricellular protein in the fasciclin family, and modulates cell-to-ECM interactions.[38,39] It is predominantly expressed in connective tissues, such as bone and tendon, and is also expressed in human IVDs.[40] As for osteoarthritis (OA), a joint degenerative disease, periostin was reported to

Figure 4. Targeting periostin attenuates IDD *in vivo*

(A) Immunoblotting results of three control and three degenerated human NP tissues. C, control; D, degenerated. (B) Representative IHC staining images of periostin and NF-κB p65 in NP tissues from patients with different degeneration grades. Scale bar, 100 μm. (C) IHC score of periostin in moderately (II and III, n = 7) and severely (IV and V, n = 8) degenerated NP tissues. (D) Pearson correlation between the periostin IHC score and the percentage of $p65^{+}$ cells in human NP tissues. n = 15. (E) Rat tail with the controlled static compressive loading apparatus (left panel), and representative T2-weighted images (T2WI) of rat tails 2 weeks after surgery (right panel). OP, operation; *GFP*, AAV2-*GFP*; si*Postn*, AAV2-*Postn*-siRNA. (F) MRI Pfirrmann grade of different groups. n = 5 biologically independent samples. (G) Representative images of H&E (upper) and Safranin O/Fast Green (bottom) staining of rat tail IVDs with indicated administration. Scale bar, 400 μm. (H and I) Representative images of p16 (H) and periostin and p65 (I) IHC staining in different groups. Scale bar, 100 μm. (J and K) Periostin IHC score (J) and $p65^{+}$ cells (%) (K) in different groups. n = 3 biologically independent samples. (L and M) Representative T2WI images (L) and MRI Pfirrmann grade (M) of rat tail IVDs treated with IgG or periostin neutralizing antibodies after operation. n = 3 biologically independent samples. Data are presented as the mean ± SD. *$p < 0.05$.

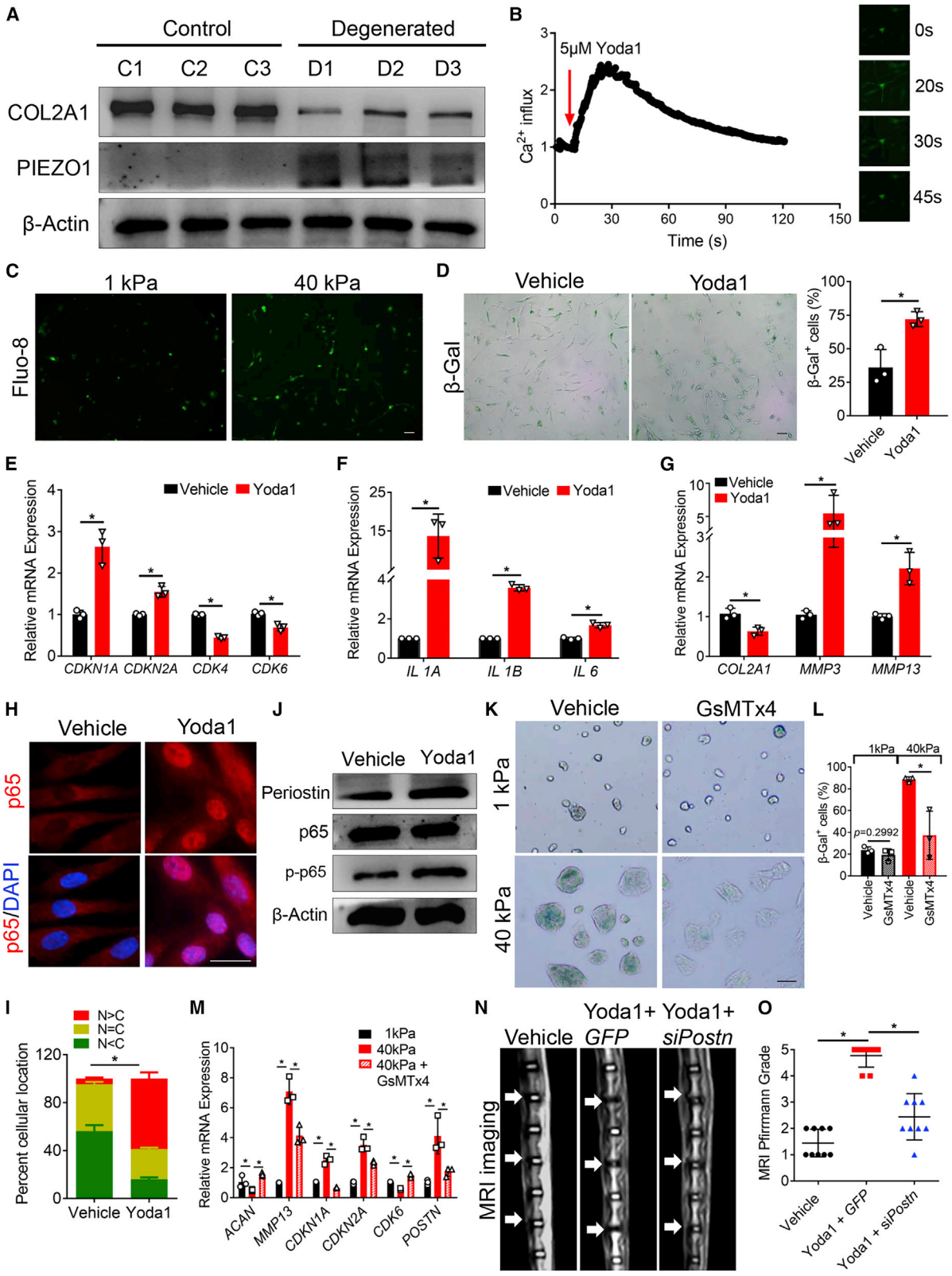

(legend on next page)

be upregulated in the damaged cartilage of an OA mouse model and OA patients.[41–44] *In vitro* experiments showed that periostin might accelerate the progression of OA via activating NF-κB p65 and upregulating pro-inflammatory factors in cultured human articular cartilage cells.[42] A recent study showed that periostin expression was increased in human degenerative IVD cells[31]; however, less was known about the role of periostin in disc loading and degeneration. Our unbiased mRNA-seq results revealed that *POSTN* expression was increased most under mechanic stimuli in hNPCs, and we also found that NF-κB p65 upregulated *POSTN* transcriptionally. Furthermore, our results showed that secreted periostin accelerated hNPCs senescence and promoted periostin secretion via activating NF-κB p65, which formed a positive feedback loop to accelerate IDD. We illustrated the mechanistic role of periostin in disc loading and IDD progression. Both *Postn* knockdown via siRNA and periostin inactivation via neutralizing antibodies attenuated IDD progression *in vivo*, suggesting that periostin was a potential therapeutic target for IDD treatment.

PIEZO1 is known to regulate diverse biological processes, such as bone development and homeostasis.[34,45] However, the function of PIEZO1 in the IVD is far from well known. Very recently, it was reported that PIEZO1 knockdown by siRNA attenuated ECM-induced hNPCs senescence and partially ameliorated the progression of IDD in puncture rat models,[20] and another study showed that activation of Piezo1 significantly upregulated catabolic metabolism.[46] In our study, we found that PIEZO1 was hardly detected in non-degenerated NP tissues by western blot, consistent with the low expression of Piezo1-tdTomato in adult mouse IVDs (Figure S5). However, treatment with the PIEZO1-specific agonist Yoda1 induced calcium influx in cultured healthy hNPCs (Figure 5B), suggesting that PIEZO1 might function and sense mechano-stress in healthy hNPCs. Furthermore, Yoda1 treatment induced periostin and p-p65 expression (Figures 5J and S3), which was reversed by BAY treatment (Figure S3), suggesting that PIEZO1 induced periostin expression via NF-κB p65. Since PIEZO1 expression in degenerated tissues was quite elevated (Figure 5A), we further examined PIEZO1 expression at 0, 6, 12, 24, and 48 h after Yoda1 treatment. Interestingly, PIEZO1 expression was elevated in a time-dependent manner after Yoda1 treatment (Figure S4). Meanwhile, Whasil Lee and her colleagues recently reported that inflammatory signaling upregulated and sensitized PIEZO1 mechanotransduction in articular chondrocytes.[47] Here, our data showed that PIEZO1 expression, as well as periostin and p-p65 expressions, was significantly increased after Yoda1 treatment, but how PIEZO1 expression was regulated under mechano-stress needs further investigation. Furthermore, whether the increased PIEZO1 expression in diseased tissues elevates the calcium baseline and renders hNPCs mechanically hypersensitive requires more investigation as well. *In vivo*, we found that Yoda1 induced IDD quickly after injection, even in the absence of physical pressure, and periostin knockdown by AAV2-si*Postn* attenuated Yoda1-induced IDD in rat tails, indicating that PIEZO1 activation triggered IDD progression via periostin.

In conclusion, our study first characterized the mechanistic role of periostin in mechano-induced hNPCs senescence and IDD progression, and further demonstrated the self-amplifying loop of NF-κB and periostin, which was initiated via PIEZO1, and was involved in accelerating hNPCs senescence and IDD progression (Figure 6). Our research revealed a new mechanism by which mechano-stress promoted senescence and SASP in IDD, and periostin neutralizing antibodies may serve as new therapeutic agents for the treatment of mechano-induced IDD.

MATERIALS AND METHODS

Hydrogel preparation and cell culture

The hydrogels with different stiffness were prepared as previously described.[34] Briefly, a solution of 40% acrylamide (Sigma-Aldrich), 2% bis-acrylamide (Sigma-Aldrich), ammonium persulfate (1:100), and TEMED (1:1000) was prepared to obtain the desired modulus of elasticity. The solution was then allowed to polymerize for 30 min, followed by cross-linking to Sulfo-SANPAH (Thermo Fisher Scientific) under 365-nm UV light at a distance of 3 inches for 10 min. The cross-linked hydrogels were coated with collagen type I (BD Biosciences) at 37°C overnight and sterilized under UV for 30 min before cells were seeded.

hNPCs and human AF cells were obtained from ScienCell and cultured in corresponding complete culture medium (ScienCell) in a humidity incubator at 37°C with 5% CO_2. BAY 11–7085 (GLPBIO, 1 μM), TNF-α (Peprotech, 10 ng/mL), recombinant human periostin (R&D, 1 μg/mL), SB-273005 (GLPBIO, 1 μM), Yoda1 (GLPBIO, 5 μM) and GsMTx4 (GLPBIO, 2 μM) were purchased from indicated companies and administrated with indicated concentration.

Figure 5. Mechano-stress initiates the positive loop of NF-κB and periostin via PIEZO1

(A) Immunoblotting results of three control and three degenerated human NP tissues. C, control; D, degenerated. (B) Quantitation of Ca^{2+} influx changes in hNPCs after 5 μM Yoda1 stimulation (left panel), and representative fluorescence images at indicated time points (right panel). Yoda1 was administrated at 10 s. (C) Representative images of Fluo-8 AM in hNPCs cultured on different hydrogels. Scale bar = 100 μm. (D) Representative β-Gal staining images of hNPCs treated with vehicle or Yoda1 for 24 h (left panel), and quantitation of β-Gal$^+$ senescent cells (right panel). n = 3 biologically independent samples. Scale bar, 100 μm. (E–G) qPCR results of senescence (E), SASP (F), and matrix metabolism (G) markers in hNPCs treated with vehicle or Yoda1 for 24 h. n = 3 biologically independent samples. (H) Representative immunostaining images of NF-κB p65 (red) in hNPCs under indicated treatments for 30 min. DAPI (blue) indicates nuclei. (I) Quantification of p65 localization in (H), presented as mean ± SD. In total, 237 cells from the vehicle group and 232 cells from the Yoda1 group were analyzed. *Represents the statistical analysis was conducted in terms of the proportion of N > C between the two groups and the $p < 0.05$. n = 3 biologically independent samples. Scale bar = 25 μm. (J) Immunoblotting results of hNPCs treated with vehicle or Yoda1 for 48 h. (K and L) Representative β-Gal staining images of hNPCs under indicated conditions for 24 h (K), and quantitation of β-Gal$^+$ senescent cells (L). n = 3 biologically independent samples. Scale bar, 100 μm. (M) Relative mRNA expression of the matrix metabolism and senescence markers and *POSTN* in hNPCs under indicated conditions. n = 3 biologically independent samples. (N and O) Representative T2WI image (N) and MRI Pfirrmann grade (O) of rat tail IVDs with indicated administration. n = 9 discs. Data are presented as the mean ± SD. *$p < 0.05$.

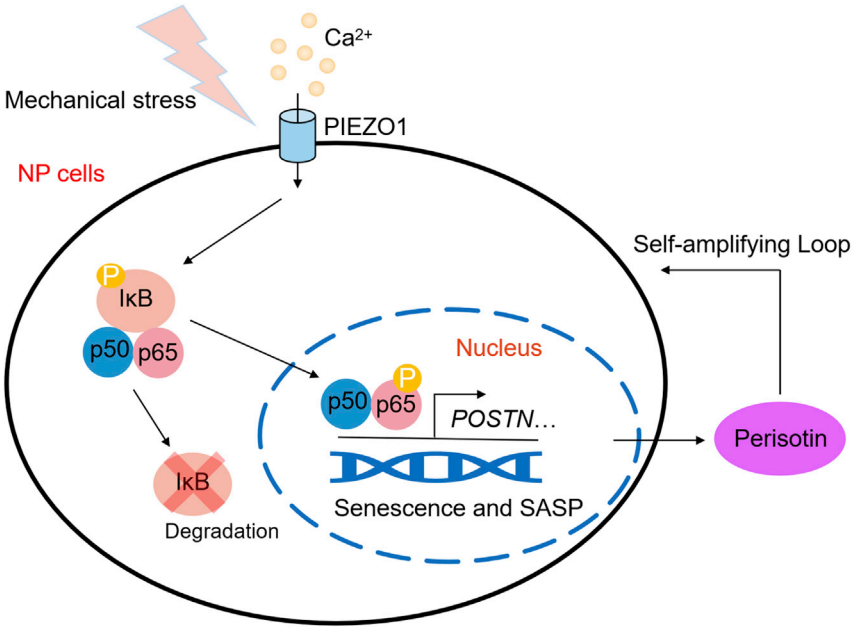

Figure 6. Proposed schematic representation of the self-amplifying loop of NF-κB and periostin accelerating mechano-induced senescence of the NP and IDD

In NPCs, mechano-stress activates NF-κB p65 via PIEZO1-Ca^{2+} to transcriptionally upregulate periostin, while the periostin secreted by senescent NPCs in turn activates NF-κB p65, forming a self-amplifying loop to accelerate senescence and IDD progression.

Senescence-associated β-galactosidase staining

Senescence-associated β-galactosidase (SA-β-gal) staining (Beyotime) was performed according to the manufacturer's protocol. In brief, cells were washed with PBS and fixed in SA-β-Gal fixative for 15 min at room temperature, followed by incubation with SA-β-Gal working solution at 37°C without CO_2 overnight. After staining, three random fields of each group were imaged under an optical microscope, and the ratio of $β\text{-}Gal^+$ cells was calculated.

Quantitative real-time polymerase chain reaction

Total RNA was extracted using TRIzol reagent (Invitrogen), and then reverse transcribed into cDNA by M-MLV Reverse Transcriptase (TaKaRa). Quantitative real-time polymerase chain reaction (qPCR) was performed using SYBR Green Real-Time PCR Master Mix (TaKaRa) following the manufacturer's instruction. The relative mRNA expression was determined by the $2^{-\Delta\Delta Ct}$ method and normalized to *GAPDH* expression. The primers used in this study were listed in Table 1.

Enzyme-linked immunosorbent assay

The culture medium of hNPCs cultured under different conditions was collected, and the concentrations of IL-1β (NeoBioscience), IL-6 (NeoBioscience), IL-8 (NeoBioscience), and periostin (Boster) were determined with human enzyme-linked immunosorbent assay (ELISA) kits according to the manufacturer's protocols.

RNA sequencing and analysis

Total RNA was extracted from hNPCs cultured on different hydrogels and libraries were generated using the VAHTS Stranded mRNA-seq Library Prep Kit for Illumina (New England Biolabs). Library quality was checked by a Bioptic Qsep100 Analyzer (Bioptic Inc.), and libraries were sequenced using a NovaSeq 6000. Genes with a fold change > 8 and $p < 0.05$ were identified as differentially expressed genes and analyzed using DAVID Bioinformatics Resources 6.8.[48,49] Two biological replicates in each group were included for the RNA sequencing (RNA-seq) experiment in the study.

Immunofluorescence staining

hNPCs seeded on cover slips were treated with indicated stimuli and then fixed with 4% paraformaldehyde for 15 min, followed by permeabilization with 0.5% Triton X-100 for 5 min. After blocking with 5% bovine serum albumin for 30 min, the slips were incubated with primary antibodies overnight at 4°C, washed, and incubated with secondary antibodies at room temperature for 1 h. The cover slips were finally mounted with Fluoroshield with DAPI (Sigma-Aldrich) and photographed under a fluorescence microscope.

ATAC-seq and analysis

hNPCs were cultured on different hydrogels for 24 h and then collected for ATAC-seq. Two replicates were prepared for each group. ATAC-seq was performed and the results were analyzed as described previously.[33] Briefly, nuclei were isolated from 50,000 cells for transposition reaction with Epi ATAC-seq kit (Epibiotek). DNA was purified with a DNA purification kit (Qiagen) and amplified with NEBNext high-fidelity 2× PCR Master Mix (New England Biolabs) to generate libraries. Libraries were quantified with a Bioptic Qsep100 Analyzer (Bioptic Inc.) and paired-end sequenced with read lengths of 150 using a NovaSeq 6000. After removing low-quality reads (quality < 15) and adapters using Cutadapt, ATAC-seq reads were mapped to the human genome (hg38) using Bowtie2. Only uniquely mapped paired reads were sorted using SAMtools and kept for subsequent analysis. Significant peak regions of each sample were identified using MACS2. Viewable bigwig files were generated using Deep tools and presented by Integrative Genomics Viewer software. The genomic region of the peak was annotated using the ChIPseeker R package. Differentially sites were detected from ATAC-seq experiments using the DiffBind R package. Ontologies of genes were identified by DAVID Bioinformatics Resources 6.8.[48,49]

CRISPRi/sgRNA plasmid construction and lentivirus infection

The pLV hU6-sgRNA hUbC-dCas9-KRAB-T2a-Puro plasmid (Addgene, #71236) was obtained from Addgene. The sgRNA

Table 1. Primers for qPCR

Gene	Primer sequence (5′-3′)
GAPDH	Forward: ACAACTTTGGTATCGTGGAAGG
	Reverse: GCCATCACGCCACAGTTTC
CDKN1A	Forward: CGATGGAACTTCGACTTTGTCA
	Reverse: GCACAAGGGTACAAGACAGTG
CDKN2A	Forward: GGGTTTTCGTGGTTCACATCC
	Reverse: CTAGACGCTGGCTCCTCAGTA
CDK4	Forward: TCAGCACAGTTCGTGAGGTG
	Reverse: GTCCATCAGCCGGACAACAT
CDK6	Forward: TCTTCATTCACACCGAGTAGTGC
	Reverse: TGAGGTTAGAGCCATCTGGAAA
IL1A	Forward: TGGTAGTAGCAACCAACGGGA
	Reverse: ACTTTGATTGAGGGCGTCATTC
IL1B	Forward: AGCTACGAATCTCCGACCAC
	Reverse: CGTTATCCCATGTGTCGAAGAA
IL6	Forward: ACTCACCTCTTCAGAACGAATTG
	Reverse: CCATCTTTGGAAGGTTCAGGTTG
CXCL8	Forward: ACTGAGAGTGATTGAGAGTGGAC
	Reverse: AACCCTCTGCACCCAGTTTTC
MMP3	Forward: CTGGACTCCGACACTCTGGA
	Reverse: CAGGAAAGGTTCTGAAGTGACC
MMP13	Forward: TCCTGATGTGGGTGAATACAATG
	Reverse: GCCATCGTGAAGTCTGGTAAAAT
ACAN	Forward: GTGCCTATCAGGACAAGGTCT
	Reverse: GATGCCTTTCACCACGACTTC
COL1A1	Forward: GAGGGCCAAGACGAAGACATC
	Reverse: CAGATCACGTCATCGCACAAC
COL2A1	Forward: TGGACGATCAGGCGAAACC
	Reverse: GCTGCGGATGCTCTCAATCT
COL3A1	Forward: GCCAAATATGTGTCTGTGACTCA
	Reverse: GGGCGAGTAGGAGCAGTTG
FN1	Forward: AGGAAGCCGAGGTTTTAACTG
	Reverse: AGGACGCTCATAAGTGTCACC
POSTN	Forward: GCTATTCTGACGCCTCAAAACT
	Reverse: AGCCTCATTACTCGGTGCAAA

sequence targeting NF-κB p65 binding site in the *POSTN* promoter region (5′-CACCGCAGTCTAAAGATGAAAAGTG-3′) was inserted into the plasmid using BsmBI sites. Lentivirus was packed using the GeneCopoeia Lenti-Pac kit (GeneCopoeia). In brief, HEK 293T cells were cultured in DMEM (Thermo Fisher Scientific) containing 10% fetal bovine serum and 1% penicillin-streptomycin. Polyethylenimine (Sigma-Aldrich) was used to co-transfect 2.5 μg dCas9 plasmid (described above) and packing plasmids (pLP1, pLP2, and pLP-vsvg) into HEK 293T cells. hNPCs were infected with lentivirus for 48 h and then treated with either Yoda1 or TNF-α for 24 h. Finally, the cells were collected for RNA extraction and qPCR analysis.

Chromatin-immunoprecipitation-quantitative real-time polymerase chain reaction

ChIP assays were performed using the Cell Signaling Technology (CST) SimpleChIP Enzymatic Chromatin IP Kit (CST, #9003). Briefly, hNPCs (1×10^7) were treated with PBS, 10 ng/mL TNF-α, or 5 μM Yoda1 for 24 h, followed by cross-linking and lysis. The sheared chromatin was incubated with anti-NF-κB p65 (CST, #6956) and magnetic protein A/G beads. IgG was used as control. The immune complexes were purified and further analyzed using qPCR for the *POSTN* promoter. qPCR results were represented as a percentage of input DNA. qPCR primers for ChIP were as follows: *POSTN* promoter Forward: 5′-AAAAGAAAGGAAATGAG-3′, Reverse: 5′-AAAACAAACTCTGGATAG-3′.

Dual-luciferase reporter assay

The reporter vector (pVG238-POSTN) containing the *POSTN* promoter (−2042 to −1 bp) and the firefly luciferase reporter gene was purchased from GeneChem. After transfection with siRNAs targeting p65 (RIBOBIO) for 48 h, the pVG238-POSTN vector was co-transfected with the internal control pRL-TK vector (Beyotime) in hNPCs using Lipofectamine 3000 (Invitrogen). After 48 h, hNPCs were treated with PBS, 10 ng/mL TNF-α, or 5 μM Yoda1 for 24 h and luciferase activity was assessed using the Luciferase Reporter Assay System according to the manufacturer's instructions (Beyotime). The siRNA sequences were listed in Table S1.

Immunoblotting

Cell lysates or tissues were prepared using RIPA buffer (Beyotime) containing protease inhibitor mixture (Roche) and quantified by a BCA protein assay kit (EpiZyme Scientific). Total cell lysates were analyzed by western blot according to standard procedures. The following primary antibodies were used: anti-PIEZO1 (Affinity Biosciences, #DF12083, 1:1000), anti-periostin (Proteintech, #66491-1-lg, 1:3000), anti-NF-κB p65 (CST, #6956, 1:1000), anti-phospho-NF-κB p65 (CST, #3033, 1:1000), anti-MMP13 (Proteintech, #18165-1AP, 1:1000), anti-COL2A1 (Abcam, #ab188570, 1:1000), anti-β-Actin (Affinity Biosciences, #AF7018, 1:1000), and anti-GAPDH (Proteintech, #60004-1-Ig, 1:3000).

Human subjects

The study was approved by the Medical Ethics Committee of the First Affiliated Hospital of Sun Yat-sen University, and signed informed consent forms were obtained from each subject before operation. In total, 18 clinical specimens (15 degenerated discs and three control discs) were collected between July 15 and September 15, 2021. Details of the specimens are shown in Table 2. The severity of disc degeneration was evaluated according to the Pfirrmann grading system.[50] Discs from patients with trauma or deformity were considered as control discs.

Immunohistochemistry

Tissue slides were immunoreacted with anti-periostin (Proteintech, #66491-1-lg, 1:500), anti-NF-κB p65 (CST, #6956, 1:400), and anti-p16 (Bioss, #bs-0740R, 1:200) and further processed according to

Table 2. Details of clinical samples

Case	Gender	Age	Affected IVD	Pfirrmann grade
1	female	68	L4/5	IV
2	female	55	L4/5	III
3	male	58	L5/S1	II
4	male	50	L4/5	III
5	female	71	L5/S1	III
6	male	53	L5/S1	IV
7	male	64	L4/5	V
8	male	41	L4/5	I
9	female	65	L5/S1	I
10	male	20	L3/4	I
11	female	63	L5/S1	IV
12	male	59	L4/5	IV
13	male	63	C3/4/5	III
14	female	48	C4/5/6	III
15	male	64	C3/4/5	IV
16	male	69	L4/5	IV
17	male	53	L4/5, L5/S1	III
18	female	69	L1-5	IV

Affected IVD: L, lumbar; S, sacral; C, cervical.

standard procedures. Immunostaining evaluations were performed independently by experimenters blinded to sample identity. The staining intensity was scored as described before.[51] Staining intensity was scored as follows: 0 (negative), 1 (weakly positive), 2 (moderately positive), and 3 (strongly positive). The percentage of positivity was also scored according to five categories: 0 (<5%), 1 (5%–25%), 2 (25%–50%), 3 (50%–75%), and 4 (>75%). The value of the percentage positive score was multiplied by the staining intensity score to generate final expression scores, which ranged from 0 to 12.

Animals

The experimental procedures were approved by the Animal Care and Use Committee of the First Affiliated Hospital of Sun Yat-sen University. A total of 30 specific pathogen-free (SPF) Sprague-Dawley rats (female, 12 weeks old) were purchased from Charles River Laboratories and housed under 12/12-h light/dark conditions. Rats were randomly assigned to different groups ($n \geq 3$ per group). The controlled static compressive loading apparatus and surgical procedures were as previously described.[52,53] Rats in the Sham group underwent surgical pin placement without the application of any external mechanical load, which was used to exclude any surgical stab injury-induced adverse effects on the subject IVDs. Two weeks after surgery, the external apparatus of each rat was uninstalled. AAV2-*eGFP*-RNAi and AAV2-*Postn*-RNAi were constructed by GeneChem, and locally injected into rat tails (10^{10} v.g/mL) 3 days before loading.

Magnetic resonance imaging

Rats from different groups were examined with magnetic resonance imaging (MRI). T2-weighted spin-echo sequences in the sagittal and horizontal planes were selected to evaluate the disc water content changes. The degeneration of discs was scored by the Pfirrmann grading system from 1 to 5 as previously described.[50]

Histological analysis

H&E staining and Safranin O/Fast Green staining were performed as previously described.[54] The slides were photographed under a light microscope (Olympus).

Calcium flux imaging

Calcium flux imaging was performed according to the manufacturer's instruction. Cultured hNPCs were incubated with 1 μM Fluo-8 AM (Sigma-Aldrich) in Hank's Balanced Salt Solution (HBSS) for 30 min at 37°C. Then cells were rinsed three times with HBSS at room temperature. Imaging was performed with a fluorescence microscope (Olympus). Fluorescence was recorded for 10 s in HBSS and then recorded for 1 min and 50 s after Yoda1 treatment (5 μM). Fluorescent images of hNPCs cultured on hydrogels were taken at 160 ms exposure time.

Statistical analysis

The experiments were performed with at least three biological replicates. The results were presented as mean ± SD. Statistical significance was determined by the two-tailed independent Student's *t* test for comparisons of two independent groups and by one-way ANOVA followed by Holm-Sidak test for multiple comparisons. In all cases, a p value of less than 0.05 was considered statistically significant. All statistical analyses were conducted with the SPSS 13.0 statistical software package.

DATA AVAILABILITY

All the raw sequencing data have been uploaded to GEO database: GSE185728.

SUPPLEMENTAL INFORMATION

Supplemental information can be found online at https://doi.org/10.1016/j.ymthe.2022.05.021.

ACKNOWLEDGMENTS

We thank all the members of the Su lab for the stimulating discussions. We appreciate the help from Shuhao Feng (Nanfang Hospital, Southern Medical University) on histology, and Wenwu Zhang (the First Affiliated Hospital of Sun Yat-sen University) on animal experiments. This work was supported by China Postdoctoral Science Foundation (2021M693630) and National Natural Science Foundation of China (92068105, 82172376 and 82102518).

AUTHOR CONTRIBUTIONS

T.Z. and P.S. designed and supervised the experiments. T.Z. and J.W. wrote the original manuscript. J.W., Y.C., and T.Z. reviewed and edited the manuscript. J.W., H.L., and S.Z. performed *in vitro*

experiments. D.Z., X.Q., T. C., D.S., and X.K analyzed the data. J.W., Y.C., and T.Z. performed the IDD model construction and histological analysis. T.Z., P.S., and Y.W. contributed to the clinical specimen collection and analysis. All authors contributed to interpret the results.

DECLARATION OF INTERESTS

The authors declare no competing interests.

REFERENCES

1. Vlaeyen, J., Maher, C.G., Wiech, K., Van Zundert, J., Meloto, C.B., Diatchenko, L., Battié, M.C., Goossens, M., Koes, B., and Linton, S.J. (2018). Low back pain. Nat. Rev. Dis. Primers *4*, 52. https://doi.org/10.1038/s41572-018-0052-1.
2. Hoy, D., March, L., Brooks, P., Blyth, F., Woolf, A., Bain, C., Williams, G., Smith, E., Vos, T., Barendregt, J., et al. (2014). The global burden of low back pain: estimates from the Global Burden of Disease 2010 study. Ann. Rheum. Dis. *73*, 968–974. https://doi.org/10.1136/annrheumdis-2013-204428.
3. Knezevic, N.N., Candido, K.D., Vlaeyen, J.W.S., Van Zundert, J., and Cohen, S.P. (2021). Low back pain. Lancet *398*, 78–92. https://doi.org/10.1016/s0140-6736(21)00733-9.
4. An, H.S., Masuda, K., and Inoue, N. (2006). Intervertebral disc degeneration: biological biomechanical factors. J. Orthop. Sci. *11*, 541–552. https://doi.org/10.1007/s00776-006-1055-4.
5. Silagi, E.S., Shapiro, I.M., and Risbud, M.V. (2018). Glycosaminoglycan synthesis in the nucleus pulposus: dysregulation and the pathogenesis of disc degeneration. Matrix Biol. *71-72*, 368–379. https://doi.org/10.1016/j.matbio.2018.02.025.
6. Roughley, P.J. (2004). Biology of intervertebral disc aging and degeneration: involvement of the extracellular matrix. Spine (Phila Pa 1976) *29*, 2691–2699. https://doi.org/10.1097/01.brs.0000146101.53784.b1.
7. Roberts, S., Evans, H., Trivedi, J., and Menage, J. (2006). Histology and pathology of the human intervertebral disc. J. Bone Joint Surg. Am. *88*, 10–14. https://doi.org/10.2106/jbjs.f.00019.
8. Lawson, L., and Harfe, B.D. (2015). Notochord to nucleus pulposus transition. Curr. Osteoporos. Rep. *13*, 336–341. https://doi.org/10.1007/s11914-015-0284-x.
9. Adams, M.A., and Roughley, P.J. (2006). What is intervertebral disc degeneration, and what causes it? Spine (Phila Pa 1976) *31*, 2151–2161. https://doi.org/10.1097/01.brs.0000231761.73859.2c.
10. Lyu, F.J., Cui, H., Pan, H., MC Cheung, K., Cao, X., Iatridis, J.C., and Zheng, Z. (2021). Painful intervertebral disc degeneration and inflammation: from laboratory evidence to clinical interventions. Bone Res. *9*, 7. https://doi.org/10.1038/s41413-020-00125-x.
11. Binch, A.L.A., Fitzgerald, J.C., Growney, E.A., and Barry, F. (2021). Cell-based strategies for IVD repair: clinical progress and translational obstacles. Nat. Rev. Rheumatol. *17*, 158–175. https://doi.org/10.1038/s41584-020-00568-w.
12. Cheng, Z., Xiang, Q., Wang, J., and Zhang, Y. (2021). The potential role of melatonin in retarding intervertebral disc ageing and degeneration: a systematic review. Ageing Res. Rev. *70*, 101394. https://doi.org/10.1016/j.arr.2021.101394.
13. Zhang, G.Z., Liu, M.Q., Chen, H.W., Wu, Z.L., Gao, Y.C., Ma, Z.J., He, X.G., and Kang, X.W. (2021). NF-κB signalling pathways in nsucleus pulposus cell function and intervertebral disc degeneration. Cell Prolif *54*, e13057. https://doi.org/10.1111/cpr.13057.
14. Newell, N., Little, J.P., Christou, A., Adams, M.A., Adam, C.J., and Masouros, S.D. (2017). Biomechanics of the human intervertebral disc: a review of testing techniques and results. J. Mech. Behav. Biomed. *69*, 420–434. https://doi.org/10.1016/j.jmbbm.2017.01.037.
15. Feng, C., Liu, H., Yang, M., Zhang, Y., Huang, B., and Zhou, Y. (2016). Disc cell senescence in intervertebral disc degeneration: causes and molecular pathways. Cell Cycle *15*, 1674–1684. https://doi.org/10.1080/15384101.2016.1152433.
16. Le Huec, J.C., Saddiki, R., Franke, J., Rigal, J., and Aunoble, S. (2011). Equilibrium of the human body and the gravity line: the basics. Eur. Spine J. *20*, 558–563. https://doi.org/10.1007/s00586-011-1939-7.
17. Zhao, R., Liu, W., Xia, T., and Yang, L. (2019). Disordered mechanical stress and tissue engineering therapies in intervertebral disc degeneration. Polymers (Basel) *11*, 1151.
18. Iatridis, J.C., Setton, L.A., Weidenbaum, M., and Mow, V.C. (1997). Alterations in the mechanical behavior of the human lumbar nucleus pulposus with degeneration and aging. J. Orthop. Res. *15*, 318–322. https://doi.org/10.1002/jor.1100150224.
19. Fearing, B.V., Jing, L., Barcellona, M.N., Witte, S.E., Buchowski, J.M., Zebala, L.P., Kelly, M.P., Luhmann, S., Gupta, M.C., Pathak, A., and Setton, L.A. (2019). Mechanosensitive transcriptional coactivators MRTF-A and YAP/TAZ regulate nucleus pulposus cell phenotype through cell shape. FASEB J. *33*, 14022–14035. https://doi.org/10.1096/fj.201802725rrr.
20. Wang, B., Ke, W., Wang, K., Li, G., Ma, L., Lu, S., Xiang, Q., Liao, Z., Luo, R., Song, Y., et al. (2021). Mechanosensitive ion channel Piezo1 activated by matrix stiffness regulates oxidative stress-induced senescence and apoptosis in human intervertebral disc degeneration. Oxid. Med. Cell. Longev. *2021*, 1–13. https://doi.org/10.1155/2021/8884922.
21. Zhang, Y., Yang, B., Wang, J., Cheng, F., Shi, K., Ying, L., Wang, C., Xia, K., Huang, X., Gong, Z., et al. (2020). Cell senescence: a nonnegligible cell state under survival stress in pathology of intervertebral disc degeneration. Oxid. Med. Cell. Longev. *2020*, 1–12. https://doi.org/10.1155/2020/9503562.
22. Roberts, S., Evans, E.H., Kletsas, D., Jaffray, D.C., and Eisenstein, S.M. (2006). Senescence in human intervertebral discs. Eur. Spine J. *15*, S312–S316. https://doi.org/10.1007/s00586-006-0126-8.
23. Novais, E.J., Diekman, B.O., Shapiro, I.M., and Risbud, M.V. (2019). p16(Ink4a) deletion in cells of the intervertebral disc affects their matrix homeostasis and senescence associated secretory phenotype without altering onset of senescence. Matrix Biol. *82*, 54–70. https://doi.org/10.1016/j.matbio.2019.02.004.
24. Risbud, M.V., and Shapiro, I.M. (2014). Role of cytokines in intervertebral disc degeneration: pain and disc content. Nat. Rev. Rheumatol. *10*, 44–56. https://doi.org/10.1038/nrrheum.2013.160.
25. Childs, B.G., Baker, D.J., Kirkland, J.L., Campisi, J., and van Deursen, J.M. (2014). Senescence and apoptosis: dueling or complementary cell fates? EMBO Rep. *15*, 1139–1153. https://doi.org/10.15252/embr.201439245.
26. Che, H., Li, J., Li, Y., Ma, C., Liu, H., Qin, J., Dong, J., Zhang, Z., Xian, C.J., Miao, D., et al. (2020). p16 deficiency attenuates intervertebral disc degeneration by adjusting oxidative stress and nucleus pulposus cell cycle. Elife *9*, e52570. https://doi.org/10.7554/elife.52570.
27. Takeshita, S., Kikuno, R., Tezuka, K., and Amann, E. (1993). Osteoblast-specific factor 2: cloning of a putative bone adhesion protein with homology with the insect protein fasciclin I. Biochem. J. *294* (Pt 1), 271–278. https://doi.org/10.1042/bj2940271.
28. Idolazzi, L., Ridolo, E., Fassio, A., Gatti, D., Montagni, M., Caminati, M., FAssio, A., InCorvaia, C., and Senna, G. (2017). Periostin: the bone and beyond. Eur. J. Intern. Med. *38*, 12–16. https://doi.org/10.1016/j.ejim.2016.11.015.
29. Walker, J.T., McLeod, K., Kim, S., Conway, S.J., and Hamilton, D.W. (2016). Periostin as a multifunctional modulator of the wound healing response. Cell Tissue Res. *365*, 453–465. https://doi.org/10.1007/s00441-016-2426-6.
30. Rios, H.F., Ma, D., Xie, Y., Giannobile, W.V., Bonewald, L.F., Conway, S.J., and Feng, J. (2008). Periostin is essential for the integrity and function of the periodontal ligament during occlusal loading in mice. J. Periodontol. *79*, 1480–1490. https://doi.org/10.1902/jop.2008.070624.
31. Tsai, T.T., Lai, P.L., Liao, J.C., Fu, T.S., Niu, C.C., Chen, L.H., Lee, M.S., Chen, W.J., Fang, H.C., Ho, N.Y., and Pang, J.H.S. (2013). Increased periostin gene expression in degenerative intervertebral disc cells. Spine J. *13*, 289–298. https://doi.org/10.1016/j.spinee.2013.01.040.
32. Adams, P.D. (2007). Remodeling of chromatin structure in senescent cells and its potential impact on tumor suppression and aging. Gene *397*, 84–93. https://doi.org/10.1016/j.gene.2007.04.020.
33. Cong, Q., Liu, Y., Zhou, T., Zhou, Y., Xu, R., Cheng, C., Chung, H.S., Yan, M., Zhou, H., Liao, Z., et al. (2021). A self-amplifying loop of YAP and SHH drives formation and expansion of heterotopic ossification. Sci. Transl. Med. *13*, eabb2233. https://doi.org/10.1126/scitranslmed.abb2233.
34. Zhou, T., Gao, B., Fan, Y., Liu, Y., Feng, S., Cong, Q., Zhang, X., Zhou, Y., Yadav, P.S., Lin, J., et al. (2020). Piezo1/2 mediate mechanotransduction essential for bone

formation through concerted activation of NFAT-YAP1-ß-catenin. Elife *9*, e52779. https://doi.org/10.7554/elife.52779.

35. Ward, C.W., Sachs, F., Bush, E.D., and Suchyna, T.M. (2018). GsMTx4-D provides protection to the D2.mdx mouse. Neuromuscul. Disord. *28*, 868–877. https://doi.org/10.1016/j.nmd.2018.07.005.

36. Zhao, X., Kong, Y., Liang, B., Xu, J., Lin, Y., Zhou, N., Li, J., Jiang, B., Cheng, J., Li, C., and Wang, W. (2022). Mechanosensitive Piezo1 channels mediate renal fibrosis. JCI Insight *7*, e152330. https://doi.org/10.1172/jci.insight.152330.

37. Molladavoodi, S., McMorran, J., and Gregory, D. (2020). Mechanobiology of annulus fibrosus and nucleus pulposus cells in intervertebral discs. Cell Tissue Res. *379*, 429–444. https://doi.org/10.1007/s00441-019-03136-1.

38. Horiuchi, K., Amizuka, N., Takeshita, S., Takamatsu, H., Katsuura, M., Ozawa, H., Toyama, Y., Bonewald, L.F., and Kudo, A. (1999). Identification and characterization of a novel protein, periostin, with restricted expression to periosteum and periodontal ligament and increased expression by transforming growth factor β. J. Bone Miner Res. *14*, 1239–1249. https://doi.org/10.1359/jbmr.1999.14.7.1239.

39. Kashima, T.G., Nishiyama, T., Shimazu, K., Shimazaki, M., Kii, I., Grigoriadis, A.E., Fukayama, M., and Kudo, A. (2009). Periostin, a novel marker of intramembranous ossification, is expressed in fibrous dysplasia and in c-Fos-overexpressing bone lesions. Hum. Pathol. *40*, 226–237. https://doi.org/10.1016/j.humpath.2008.07.008.

40. Gruber, H.E., Norris, R.A., Kern, M.J., Hoelscher, G.L., Ingram, J.A., Zinchenko, N., and Hanley, E. (2011). Periostin is expressed by cells of the human and sand rat intervertebral discs. Biotech. Histochem. *86*, 199–206. https://doi.org/10.3109/10520291003722774.

41. Attur, M., Duan, X., Cai, L., Han, T., Zhang, W., Tycksen, E.D., Samuels, J., Brophy, R.H., Abramson, S.B., and Rai, M.F. (2021). Periostin loss-of-function protects mice from post-traumatic and age-related osteoarthritis. Arthritis Res. Ther. *23*, 104. https://doi.org/10.1186/s13075-021-02477-z.

42. Chijimatsu, R., Kunugiza, Y., Taniyama, Y., Nakamura, N., Tomita, T., and Yoshikawa, H. (2015). Expression and pathological effects of periostin in human osteoarthritis cartilage. BMC Musculoskelet. Disord. *16*, 215. https://doi.org/10.1186/s12891-015-0682-3.

43. Attur, M., Yang, Q., Shimada, K., Tachida, Y., Nagase, H., Mignatti, P., Statman, L., Palmer, G., Kirsch, T., Beier, F., and Abramson, S.B. (2015). Elevated expression of periostin in human osteoarthritic cartilage and its potential role in matrix degradation via matrix metalloproteinase-13. FASEB J. *29*, 4107–4121. https://doi.org/10.1096/fj.15-272427.

44. Han, T., Mignatti, P., Abramson, S.B., and Attur, M. (2020). Periostin interaction with discoidin domain receptor-1 (DDR1) promotes cartilage degeneration. PLoS One *15*, e0231501. https://doi.org/10.1371/journal.pone.0231501.

45. Wang, L., You, X., Lotinun, S., Zhang, L., Wu, N., and Zou, W. (2020). Mechanical sensing protein PIEZO1 regulates bone homeostasis via osteoblast-osteoclast crosstalk. Nat. Commun. *11*, 282. https://doi.org/10.1038/s41467-019-14146-6.

46. Sun, Z., Zheng, X., Li, S., Zeng, B., Yang, J., Ling, Z., and Fuxin, W. (2021). Single impact injury of vertebral endplates without structural disruption, initiates disc degeneration through Piezo1 mediated inflammation and metabolism dysfunction. Spine (Phila Pa 1976) *47*, E203–E213.

47. Lee, W., Nims, R.J., Savadipour, A., Zhang, Q., Leddy, H.A., Liu, F., McNulty, A.L., Chen, Y., Guilak, F., and Liedtke, W.B. (2021). Inflammatory signaling sensitizes Piezo1 mechanotransduction in articular chondrocytes as a pathogenic feed-forward mechanism in osteoarthritis. Proc. Natl. Acad. Sci. U S A *118*. e2001611118. https://doi.org/10.1073/pnas.2001611118.

48. Huang, D.W., Sherman, B.T., Tan, Q., Kir, J., Liu, D., Bryant, D., Guo, Y., Stephens, R., Baseler, M.W., Lane, H.C., and Lempicki, R.A. (2007). DAVID Bioinformatics Resources: expanded annotation database and novel algorithms to better extract biology from large gene lists. Nucleic Acids Res. *35*, W169–W175. https://doi.org/10.1093/nar/gkm415.

49. Huang, D.W., Sherman, B.T., and Lempicki, R.A. (2009). Systematic and integrative analysis of large gene lists using DAVID bioinformatics resources. Nat. Protoc. *4*, 44–57. https://doi.org/10.1038/nprot.2008.211.

50. Pfirrmann, C.W.A., Metzdorf, A., Zanetti, M., Hodler, J., and Boos, N. (2001). Magnetic resonance classification of lumbar intervertebral disc degeneration. Spine (Phila Pa 1976) *26*, 1873–1878. https://doi.org/10.1097/00007632-200109010-00011.

51. Lian, C., Wang, X., Qiu, X., Wu, Z., Gao, B., Liu, L., Liang, G., Zhou, H., Yang, X., Peng, Y., et al. (2019). Collagen type II suppresses articular chondrocyte hypertrophy and osteoarthritis progression by promoting integrin β1−SMAD1 interaction. Bone Res. *7*, 8. https://doi.org/10.1038/s41413-019-0046-y.

52. Lotz, J.C., Colliou, O.K., Chin, J.R., Duncan, N.A., and Liebenberg, E. (1998). Compression-induced degeneration of the intervertebral disc: an in vivo mouse model and finite-element study. Spine (Phila Pa 1976) *23*, 2493–2506. https://doi.org/10.1097/00007632-199812010-00004.

53. Yurube, T., Nishida, K., Suzuki, T., Kaneyama, S., Zhang, Z., Kakutani, K., Maeno, K., Takada, T., Fujii, M., Kurosaka, M., and Doita, M. (2010). Matrix metalloproteinase (MMP)-3 gene up-regulation in a rat tail compression loading-induced disc degeneration model. J. Orthop. Res. *28*, 1026–1032. https://doi.org/10.1002/jor.21116.

54. Yadav, P.S., Feng, S., Cong, Q., Kim, H., Liu, Y., and Yang, Y. (2021). *Stat3* loss in mesenchymal progenitors causes Job syndrome–like skeletal defects by reducing Wnt/β-catenin signaling. Proc. Natl. Acad. Sci. U S A *118*. e2020100118. https://doi.org/10.1073/pnas.2020100118.